Proceedings of the Combustion Institute, Volume 28, 2000/pp. 123–131

PROBABILITY DENSITY FUNCTION COMPUTATIONS OF A STRONGLY SWIRLING NONPREMIXED FLAME STABILIZED ON A NEW BURNER

A. R. MASRI,[1] S. B. POPE[2] AND B. B. DALLY[3]
[1]*Department of Mechanical and Mechatronic Engineering*
University of Sydney
Sydney, NSW 2006, Australia
[2]*Department of Mechanical and Aerospace Engineering*
Cornell University
Ithaca, NY 14850, USA
[3]*Department of Mechanical Engineering*
University of Adelaide
Adelaide, SA 5005, Australia

Turbulent nonpremixed swirl-stabilized flames are common in practical combustors and form the next level of complexity after piloted and bluff-body stabilized flames. Modeling swirling flows remains a challenge especially when the swirl level is high enough to induce vortex breakdown and recirculation. This paper presents experimental results on the velocity field and the stability characteristics of a new swirl burner which has well-defined boundary conditions. This burner is capable of stabilizing turbulent nonpremixed flames which have high swirl numbers and which may have a significant degree of turbulence–chemistry interactions. A Monte Carlo–based probability density function (PDF) method is also used to compute the same turbulent, highly swirling flame using the simplest models for velocity (SLM), turbulent frequency (JPM), and molecular mixing (IEM). A single flamelet library is used here to represent chemistry. These simple computations reproduce the correct flow structure and compare well with the measured velocity field. Refinements to the computations and more extensive measurements in such flows are forthcoming.

Introduction

Swirl burners of gaseous as well as liquid fuels are currently used in a wide range of applications such as engines, turbines, furnaces, gasifiers, and boilers. When of sufficient strength, swirl will produce a large adverse pressure gradient in the direction of the flow, which leads to vortex breakdown and flow reversal. The recirculation zone, which then forms, carries back to the burner's exit plane hot combustion products which act as a stabilizing source for the flame. The recirculating vortex may be associated with an unsteady precessing motion which remains incompletely understood in both reacting and nonreacting flows [1,2]. Despite these possible instabilities, swirl combustors have the added advantage of improved combustion efficiency, better ignition stability, and reduced emissions of pollutants. These positive effects are believed to result from improved mixing rates due to enhanced turbulence levels [3].

Early studies of swirling, flows have focused on understanding the complex nature of their stability and fluid dynamics. Designs of experimental burners varied considerably, and the available measurements were limited to flowfields and mean compositions [4–12]. Although an improved picture of swirling flows has emerged from these studies, many important areas remain vague and require further research. Vortex breakdown, and the ensuing formation of a recirculation zone, remains a poorly understood phenomenon. The structure of the recirculation zones(s) which are critical for flame stabilization is not yet resolved. Transient effects of localized extinction and reignition processes on the structure of swirling flames are very important for modeling such flows. Little or no measurements of temperature and composition fields exist in swirling flows with such dominant finite-rate chemistry effects. Issues of pollutant formation remain unclear despite the common perception that such flames lead to lower emissions of oxides of nitrogen (NO_x).

Recent progress in modeling and computational capabilities have put a number of advanced numerical methods within reach of computing finite-rate chemistry effects in turbulent reacting flows [13–15]. Xu and Pope [16] have recently advanced the probability density function (PDF) approach to compute local extinction and reignition in pilot-stabilized turbulent diffusion flames. The International Workshop on Measurement and Computation of Turbulent Nonpremixed Flames is bringing together numerical and experimental efforts to advance knowledge and

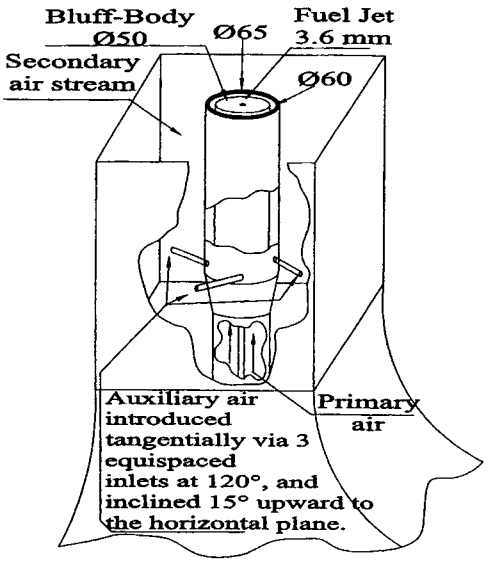

FIG. 1. Schematic of the new swirl burner.

computational capabilities in turbulent nonpremixed combustion [17]. Both piloted and bluff-body stabilized flow are adopted as model problems for this workshop series. Swirl flows form the next level of complexity in approaching model problems which closely resemble practical combustors. A good swirl burner which forms a focus for further experimental and numerical studies must (1) have strong enough swirl to cause vortex breakdown and recirculation, (2) have simple well-defined boundary conditions, (3) be amenable to laser diagnostic methods, and (4) have a region of the flame where the interaction between turbulence and chemistry is significant.

This paper is the first report from a continuing project which aims at developing an improved quantitative understanding of the structure of swirling nonpremixed flames and providing a comprehensive data bank which may be used as a benchmark for model validation. The specific objectives of this paper are

- To outline a new design for a simple swirl burner which forms an ideal model problem for investigating the complexities of swirl-stabilized flows. Another swirl burner that is currently under investigation is the Tecflam burner for which detailed experimental data are starting to appear [18,19]. We believe, however, that the burner configuration presented here has simpler boundary conditions, is more amenable to laser diagnostics, and is more appropriate for investigating basic issues of turbulence–chemistry interactions.
- To report the stability characteristics of the burner and some initial measurements of the velocity and turbulence fields.
- To demonstrate the capability of the PDF approach, using the simplest submodels, to predict the correct flow structure in such complex fields.

Burner Design and Stability Characteristics

A schematic of the new swirl burner used in this study is shown in Fig. 1. It has a 50 mm diameter bluff-body (D_B = 50 mm) with a 3.6 mm central fuel jet. Surrounding the bluff-body is a 60 mm diameter annulus for the primary swirling air stream. Swirl is introduced into the primary air stream by three tangential inlets, each 7 mm in diameter, which are positioned 150 mm upstream of the burner exit plane and inclined 15° upward to the horizontal plane. The swirl number may be easily varied by changing the relative flowrates of tangential and axial air in the primary stream. The burner assembly is situated in a wind tunnel providing a coflowing secondary air stream of 20 m/s with a free stream turbulence level of around 2%. The wind tunnel has an exit cross section of 150 × 150 mm. The fuel used is compressed natural gas (CNG) which is more than 90% methane by volume, the remaining components being primarily carbon dioxide, propane, and ethane.

Stability Characteristics

There are at least three parameters which control the stability characteristics and the physical properties of the flame: the bulk fuel jet velocity $\langle U_j \rangle$ and the bulk axial and tangential velocities in the primary air stream, $\langle U_s \rangle$ and $\langle W_s \rangle$, respectively. The coflow velocity in the secondary air stream, $\langle U_e \rangle$, may also influence the flame. In this paper, two parameters, $\langle U_s \rangle$ and $\langle U_e \rangle$ are kept constant at 33.2 and 20 m/s respectively, while $\langle U_j \rangle$ and $\langle W_s \rangle$ are varied. Stability characteristics for CNG flames are presented in Fig. 2 with respect to the geometric swirl number S_g and the momentum flux ratio of jet fuel to axial primary air

$$\frac{\rho_j \langle U_j \rangle^2}{\rho_a \langle U_s \rangle^2}$$

Here ρ_j and ρ_a are the densities of fuel and air, respectively. The geometric swirl number S_g is defined as the ratio of the tangential over the axial flowrate in the primary air stream. The solid line represents a best fit for the experimental data. Blow off occurs for flames above the solid line, and this is defined as the condition at which the flame starts to break intermittently. This may happen either at the base of the bluff body or in the neck region which occurs downstream of the recirculation zone.

For a swirl number of zero, the flame characteristics are similar to those stabilized on a bluff body [20]. The flame is about 1 m long and consists of a

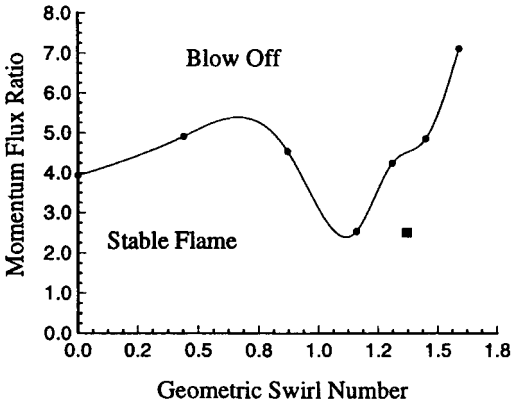

FIG. 2. Stability diagram for the swirl flame showing the fuel to primary air momentum flux ratio

$$\left(\frac{\rho_j\langle U_j\rangle^2}{\rho_a\langle U_s\rangle^2}\right)$$

versus geometric swirl number S_g. The solid line represents the best fit for the blowoff limit. Blowoff occurs above the solid line. Flames below the solid line are stable. The square shows the flame selected for further investigations.

recirculation zone on the bluff-body face and a neck zone further downstream where extinction occurs. At a fixed, non-zero swirl number and at low momentum flux ratio, the flow is dominated by the coflowing air, and the fuel is engulfed within the recirculation zone and burns on the face of the bluff-body. As its flowrate increases, the fuel penetrates the recirculation zone and burns in a jetlike manner. Further increase in the fuel flow rate eventually causes flame extinction. In the region where the geometric swirl number is between 0.8 and 1.2, the swirling flame is less stable than the standard bluff-body flame. It is believed that transition to vortex breakdown is occurring in this range of swirl number, causing the flame to become less stable. At higher swirl, the flame shortens to about 0.2 m in visible length, becomes more stable, and blows off in the neck region, while the recirculation zone further upstream remains alight. It should be noted that the computations presented here are for steadily burning flames far from blow off.

Velocity Measurements

The velocity measurements are taken using a standard Aerometrics two-dimensional laser Doppler velocimetry (LDV) system and a 4 W argon ion laser. The measurements are performed in two stages. First, the axial u and radial v components are measured, and then the same flames are scanned at the same axial locations but in a different direction such that the axial u and tangential w components of velocity are now measured. This gives mean velocities $\langle U\rangle$, $\langle V\rangle$, $\langle W\rangle$ and root mean square (rms) fluctuations, u', v', and w'. Also, shear stresses $\langle uv\rangle$ and $\langle vw\rangle$ may be obtained as well (but these are not presented here). The seeding used is submicron particles of magnesium oxide powder fed through the primary air as well as the main fuel. The error associated with the velocity measurements is of the order of 4.0%.

PDF Computations

The numerical approach is based on the transport equation for the joint PDF of velocity, composition, and turbulent frequency. A Lagrangian method is used to solve the Eulerian PDF transport equation, and stochastic differential equations (SDEs) are formed to model particle properties for velocity, dissipation, and molecular mixing terms. The SDEs are solved by a pseudo-time marching scheme over a time step, Δt. The simplified Langevin model (SLM) [15] is used for velocity, and the Jayesh–Pope model (JPM) is used for turbulent frequency [21]. A simple steady flamelet model is used so that the only composition considered is mixture fraction ξ. Molecular mixing is represented here by the simple IEM model (interaction by exchange with the mean). Further details of these models may be found elsewhere [15,22]. The code solves the PDF equations for plane and axisymmetric, statistically two-dimensional flows. It uses a particle-mesh numerical method where the solution domain is divided into a number of cells in the x and y direction (M_x and M_y, respectively), and the the fluid within each cell is represented by a number of stochastic particles, N_{pc}. An elliptic flow algorithm is used to determine the mean pressure field which is used in the velocity equation while ensuring that the mean conservation equations of mass and momentum are satisfied. A rectangular grid is used here, and the mean properties are determined for each grid node. The instantaneous properties are carried by stochastic particles within each cell.

Boundary Conditions

Figure 3 shows the boundary conditions used for selected fields of mean axial velocity $\langle U\rangle$ and its variance, mean tangential velocity $\langle W\rangle$, the mean mixing frequency $\langle\omega\rangle$, and the shear stresses $\langle uv\rangle$ and $\langle vw\rangle$ at the exit plane of the burner. Details of the boundary conditions used in the fuel jet, primary, and secondary air streams are given below.

Mean velocities

In the fuel jet, $\langle V\rangle = \langle W\rangle = 0$, and the mean axial velocity is specified by a modified power law of the form

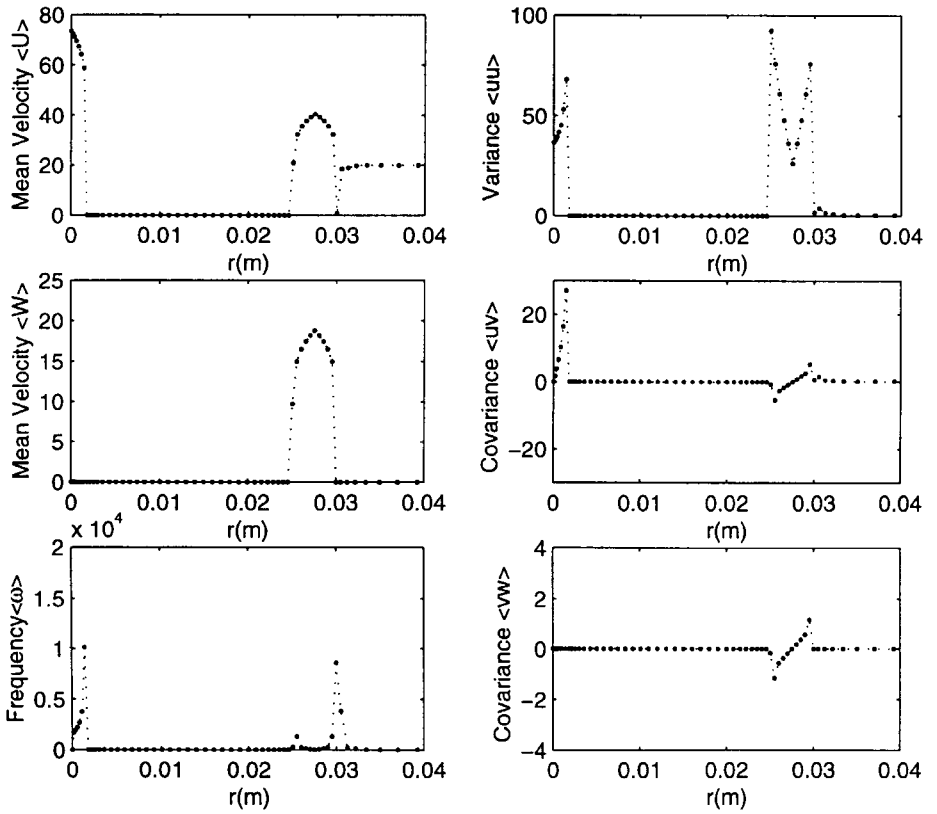

FIG. 3. Boundary conditions at the exit plane of the swirl burner. Shown are radial profiles for the mean axial and tangential velocities $\langle U\rangle$ and $\langle W\rangle$, variance of the axial velocity $\langle uu\rangle$, mean mixing frequency $\langle\omega\rangle$, and shear stresses $\langle uv\rangle$ and $\langle vw\rangle$. All quantities are in SI units.

$$\langle U\rangle = 1.218\ U_j \left(1 - \frac{|y|}{\delta}\right)^n \qquad (1)$$

where $n = 1/7$, U_j is the bulk fuel jet velocity (here $U_j = 60.3$ m/s), y is the radial distance from the jet centerline, and $\delta = 1.01 \times R_j$ where R_j is the fuel jet radius of 1.8 mm. The factor of 1.01 is added so that the velocity gradients are finite at the walls.

In the primary swirling air stream, $\langle V\rangle = 0$, and the mean axial and tangential velocities are specified as per equation 1, with y being the radial distance from the center of the annulus and $\delta = 1.01$ times the half width of the annulus. The bulk axial and tangential velocities in the swirl annulus are 33.2 and 15.4 m/s, respectively. In the secondary air stream, measured values are used for the mean axial velocity [23] and $\langle V\rangle = \langle W\rangle = 0$.

Normal and shear stresses

Measured values of $\langle uu\rangle$ are taken in the fuel jet and in the secondary air stream [23]. It is also assumed that $\langle vv\rangle = \langle ww\rangle = 0.5\ \langle uu\rangle$. The shear stresses are specified as follows, but note that the shear stresses in the secondary air stream were incorrectly specified as $\langle uv\rangle = +0.4\langle uu\rangle$. This is not expected to affect the results since, in another set of calculations, no effects were observed when the shear stresses in the boundary conditions were changed by a factor of four.

$$\text{in the fuel jet } \langle uv\rangle = 0.5\,\frac{y}{R_j}\,\langle uu\rangle \qquad (2)$$

$$\text{in the secondary air stream } \langle uv\rangle = -0.4\langle uu\rangle \qquad (3)$$

where y is radial distance from the centerline. It is also assumed that in both the fuel jet and the secondary air stream, $\langle uw\rangle = \langle vw\rangle = 0$.

In the primary air stream, rms fluctuations u' and w' are assumed to increase linearly with radial distance from the center of the annulus, $|y|$. Specified values for u' and w' are 5.11 m/s and 2.37 m/s at the center of the annulus, and these increase respectively to 9.61 m/s and 4.46 m/s at the walls. It is assumed that $v' = w'$. The shear stresses at the walls of the swirl annulus are taken as $\langle uv\rangle_w = 0.0025\ U_0^2$ and $\langle vw\rangle_w = 0.0025\ W_0^2$ where U_0 and

W_0 are the mean axial and tangential velocities in the center of the annulus. The shear stresses are then assumed to vary lineraly across the annulus from $-\langle uv\rangle_w$ and $-\langle vw\rangle_w$ at the inner wall to $+\langle uv\rangle_w$ and $+\langle uv\rangle_w$ at the outer wall. It is also assumed that $\langle uw\rangle = 0$ across the annulus.

Mean turbulent frequency

The mean turbulent frequency in the fuel jet and in the secondary air stream is taken as

$$\langle\omega\rangle = 0.27 \left|\frac{\partial\langle U\rangle}{\partial y}\right| \tag{4}$$

where y is the radial distance. In the primary swirling air stream, the mean turbulent frequency is given by $\langle\omega\rangle = \gamma P/k$ where γ is a factor taken here as 0.25, k is the turbulent kinetic energy, and P is the production which is specified as

$$P = -\left(\langle uv\rangle \frac{\partial\langle U\rangle}{\partial y} + \langle uw\rangle \frac{\partial\langle W\rangle}{\partial y}\right) \tag{5}$$

It should be appreciated that there is considerable uncertainty in the specifications of the boundary conditions. It is, of course, desirable to have measured profiles at the burner's exit plane. Such measurements are forthcoming.

Calculations were performed with different profiles for the turbulence levels, shear stresses, and mean mixing frequency at the burner's exit plane. The computed results for the mean velocity and rms fluctuations are very sensitive only to the initial mean frequency profiles and are much less sensitive to other parameters. A fourfold change in the shear stresses made almost no difference to the computed results. However, changing the mean turbulent frequency by decreasing the factor γ from 1.0 to 0.25 leads to an increase of about 30% in the calculated peak rms fluctuations u'. It should also be noted that the computed peak values of u' remain somewhat lower than the measurements, as will be shown later. On this basis, the value of $\gamma = 0.25$ was selected for the calculations reported hereon.

Numerical Issues

In a thorough investigation of the numerical issues associated with the convergence of particle-mesh algorithms for PDF methods, Xu and Pope [22] have identified three sources of numerical error. (1) Statistical error due to the number of particles representing the joint PDF being finite. This error approaches zero as $N^{-0.5}$. (2) Bias which is a deterministic error in the mean moments resulting from the statistical error. Bias scales with N^{-1}. (3) Discretization error, which is also deterministic and is due to a finite time step Δt and a finite cell size $(\Delta x, \Delta y)$. A necessary and underlying prerequisite to numerical convergence is that statistically stationary solutions are obtained.

Xu and Pope [22] proposed the following scheme to obtain numerically accurate solutions.

1. Apply time averaging after statistical stationarity is reached. This reduces the statistical error by a factor of $(2\tau/T_t)^{0.5}$ where T_t is the total time over which time averaging is performed and τ is a time scale which is proportional to the local time scale determined by the inverse of the mean frequency.
2. To reduce the deterministic error, perform two, preferably three, independent calculations with different sets of numerical parameters such that

$$\alpha \equiv \frac{M_1^2}{N_1} = \frac{M_2^2}{N_2} = \frac{M_3^2}{N_3} > 1 \tag{6}$$

The parameters α and M_i are chosen such that all solutions are in the asymptotic range of convergence of the method.

3. Use these calculations to apply a Richardson extrapolation to obtain a numerically accurate solution for the mean fields which corresponds to very large values of N and M. The scheme adopted in this paper uses three independent calculations to obtain the extrapolated solution.

Numerical and Experimental Conditions

The flame selected here for further investigation had a bulk jet velocity of 60.3 m/s, which corresponds to a Reynolds number, based on the fuel jet diameter ($D_j = 3.6$ mm) of 12,800. The fuel used was CNG. In the primary, swirling air stream, the bulk axial and tangential velocities were 33.2 m/s and 15.4 m/s, respectively. The axial velocity in the secondary air stream was 20 m/s, and the visible length of the flame was about 0.2 m. The selected flame was stable and was about 50% away from blow off, as indicated by the square symbol on the stability diagram shown in Fig. 2. Chemistry was represented in the PDF calculations using the computed structure of a steady laminar flamelet of CH_4, which has an intermediate strain rate of 200/s and a peak flame temperature of 1920 K. The laminar flamelet composition was computed as a function of mixture fraction only. A single strain rate was used throughout the computations, and no account was made for thermal radiation. The flow was axisymmetric around the fuel jet centerline, and the size of the solution domain was $x = 1000$ mm and $y = 150$ mm. The axial domain was intentionally taken to be long to prevent any feedback from the exit conditions. The solution was monitored on each time step at six sensitive locations in the flowfield to ensure that statistical stationarity was reached all over the solution domain. One monitoring point, at the centerline of the exit plane, ensured that there was no

TABLE 1
Numerical parameters used in the swirl flame calculations

	Swirling Flame Runs		
	Case 1	Case 2	Case 3
Cells in $x \times y$ directions	50×50	60×60	70×70
Particles per cell N_{pc}	208	300	408
Total steps	12,000	14,000	17,000
Start of time averaging at	8,000	9,500	12,000
Average time-step size (μs)	10.12	8.03	6.51
Average CPU time per step (s)	16.8	53.4	75.1

backflow from the outflow boundary. Standard constants were used with the simple SLM, JPM, and IEM models, and the numerical values used are given below:

C_0	$C_{\omega 1}$	$C_{\omega 2}$	$C_{\omega 3}$	$C_{\omega 4}$	$C_{\omega 5}$	C_ϕ
2.1	0.562	0.9	1.0	0.25	0.2	2.0

All computations were performed on Intel machines. Calculations were repeated for three different numbers of cells, M_i, and number of particles per cell, N_{pc} such that

$$\alpha = \frac{M_1^2}{N_1} = 12$$

This is adequate such that all calculations are in the asymptotic range. Various parameters and computational requirements for each calculation are given in Table 1.

Results and Discussion

Figure 4 shows measured and computed radial profiles for the mean and rms fluctuations of the axial

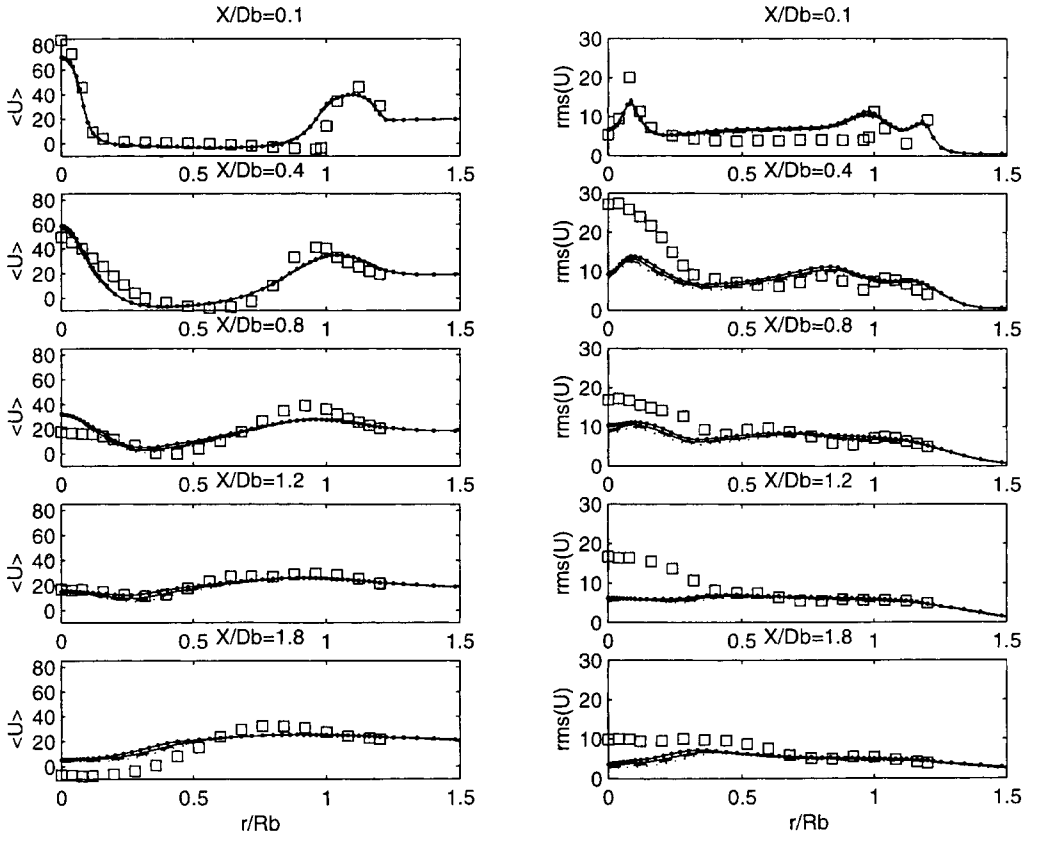

FIG. 4. Measurements and computations of mean axial velocity and its rms fluctuations at various axial locations in the swirl flame. Squares, measurements; ——, calculations 70 × 70 cells (case 3); – – –, calculations 60 × 60 cells (case 2); · · ·, calculations 50 × 50 cells (case 1); —·—, Richardson extrapolation. Units of velocity are m/s.

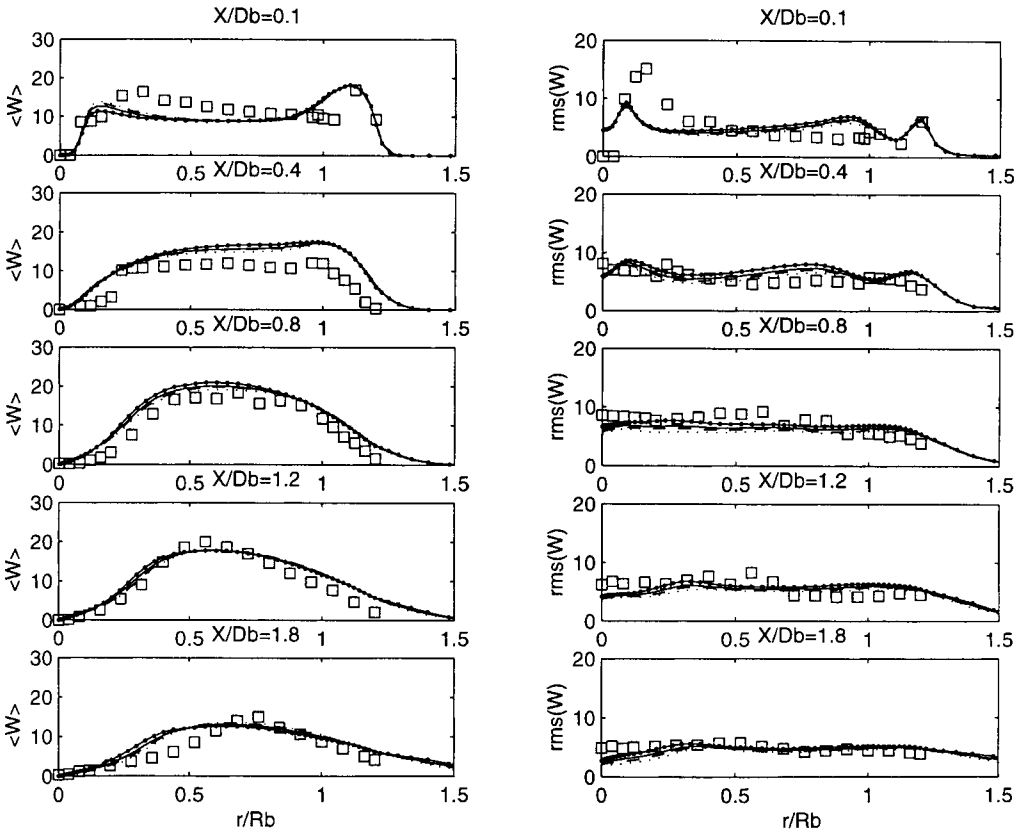

FIG. 5. Measurements and computations of mean tangential velocity and its rms fluctuations at various axial locations in the swirl flame. Squares, measurements; ——, calculations 70 × 70 cells (case 3); – – –, calculations 60 × 60 cells (case 2); · · ·, calculations 50 × 50 cells (case 1); –·– Richardson extrapolation. Units of velocity are m/s.

velocity at various axial locations in the flame. Four computed profiles are shown on each plot: three for each of cases 1, 2, and 3, and the fourth profile is obtained from the Richardson extrapolation. Comparisons are presented for $x/D_b = 0.1, 0.4, 0.8, 1.2$, and 1.8.

Although there are differences on and near the jet centerline, the mean axial velocity is computed adequately at outer radial locations. The first recirculation zone, which seems to be centered around $r/R_b \sim 0.4$ and extends for about one bluff-body diameter downstream of the burner's exit plane, is reproduced correctly in the computations. R_b is the bluff-body radius ($R_b = 25$mm). At $x/D_b = 1.8$, the negative mean axial velocities measured on and close to the centerline indicate that a second recirculation zone exists further downstream. This aspect is not reproduced adequately by the calculations. The rms fluctuations of the axial velocity are significantly underpredicted on and close to the centerline for all axial locations shown here. At larger radial locations, the rms levels decrease and are very close to the computations.

Figure 5 shows measured and computed radial profiles for the mean and rms fluctuations of the tangential velocity at various axial locations in the flame. As in Fig. 4, four computed profiles are shown on each plot, with the fourth profile being obtained from the Richardson extrapolation. Comparisons are also presented for $x/D_b = 0.1, 0.4, 0.8, 1.2$, and 1.8.

Both mean and rms fluctuations of the tangential velocity compare very well with the measurements at all axial locations shown here. At $x/D_b = 0.1$, the rms fluctuations of the tangential velocity are underpredicted, but the high levels of swirl measured right across the face of the bluff body are reproduced well by the calculations. This implies that the first recirculation zone is rotating around the jet centerline at an average of about 10 m/s. Consistent with the axial velocity, the centerline rms fluctuations are also underpredicted, but to a lesser extent.

Discussion

The swirling flame discussed here is stable and shows a complex flow pattern as expected for such a

flow geometry. Downstream of the first recirculation zone, which is located near the jet exit plane, there exists a neck region of the flame where the interaction between turbulence and chemistry becomes significant as flame blow off is approached. This neck region, unlike that in bluff-body stabilized flames, has a complex flow pattern with a second recirculation zone that lies closer to the centerline and has a high degree of swirl. The entire flame is very short and shows no soot formation, which is a necessary requirement for future laser diagnostics.

It may be seen from Figs. 4 and 5 that the differences in the results from the calculations on the three different grids are, in general, quite small. The Richardson-extrapolated values can therefore be treated as accurate numerical solutions to the modeled PDF equations.

The success of this modeling study is very encouraging considering that this is the first time that full PDF methods have been applied to strongly swirling flows. Earlier PDF computations of swirling flames have been mainly restricted to moderate swirl levels [24]. The fact that the flow structure is computed adequately reinforces the view that this geometry is well suited for further studies. Moreover, there is significant scope for improving the PDF computations by using more advanced velocity models such as Lagrangian isotropization of production model (LIPM) and mixing models such as Euclidean minimum spanning tree (EMST) [25] as well as detailed chemical kinetics. It should be noted here that using detailed chemical kinetics with the PDF approach is already possible through the use of *In situ* adaptive tabulation (ISAT) methods [26]. This has already been demonstrated successfully for pilot-stabilized flames [27–29].

Conclusions

- A new swirl-stabilized burner was introduced as a platform for further experimentation and modeling of swirl-stabilized turbulent nonpremixed flames.
- The flowfield measurements presented here for a selected flame with strong swirl showed a complex flow pattern with two recirculation zones, one near the bluff body and another further downstream in the neck region. Both recirculation zones were swirling at a high tangential velocity.
- The stability characteristics of the burner showed that, at sufficiently high swirl, the flames were more stable than bluff-body stabilized flames, were much shorter, and may blow off in the neck region downstream of the first recirculation zone. This is the region where the interaction between turbulence and chemistry is most significant.
- PDF–Monte Carlo computations of these flows using flamelet chemistry and the simplest models for velocity (SLM), frequency (JPM), and mixing (IEM) produced a flowfield that compares well with the measurements. This provides a strong incentive that the PDF approach, when applied with more advanced models and detailed chemistry, has a better chance of computing the correct compositional structure of these complex flames even when close to blow off.

Acknowledgments

This work was supported in part by the Australian Research Council and in part by the U.S. Department of Energy. Grant number DE-FG02-90ER 14128. The computational work was performed while Prof. Masri was at study leave at Cornell. The authors are grateful to Dr. J. Xu, Mr. Q. Tang and Mr. K. Liu for providing Matlab scripts for plotting.

REFERENCES

1. Leibovich, S., *AIAA J.* 22:1192–1206 (1983).
2. Syred, N., and Beer, J. M., *Combust. Flame* 22:143–201 (1974).
3. Hill, P. G., and Zhang, D., *Prog. Energy Combust. Sci.* 20:373–429 (1994).
4. Brum, R. D., and Samuelsen, G. S., *Exp. Fluids* 5:95–102 (1987).
5. Claypole, T. C., and Syred, N., *Proc. Combust. Inst.* 18:81–89 (1980).
6. Boardman, R. D., Eatough, C. N., Germane, G. J., and Smoot, L. D., *Combust. Sci. Technol.* 93:193–210 (1993).
7. Philipp, M., Hoffmann, S., and Eickhoff, H., *Proc. Combust. Inst.* 24:361–368 (1992).
8. Takahashi, F., Vangsness, M. D., Durbin, M. D., and Schmoll, W. J., *J. Heat Transfer* 118:877–884 (1996).
9. Boardman, R. D., Eatough, C. N., Germane, G. J., and Smoot, L. D., *Combust. Sci. Technol.* 93:193–210 (1993).
10. Tersaki, T., and Hayashi, S., *Proc. Combust. Inst.* 26:2733–2739 (1996).
11. Feikema, D., Chen, R. H., and Driscoll, J. F., *Combust. Flame* 80:183–195 (1990).
12. Tangirala, V., and Driscoll, J. F., *Combust. Sci. Technol.* 60:143–162 (1988).
13. Cook, A. W., and Riley, J. J., *Combust. Flame* 112:593–606 (1998).
14. Klimenko, A. Y., and Bilger, R. W., *Prog. Energy Combust. Sci.* 25:595–687 (1999).
15. Pope, S. B., *Prog. Energy Combust. Sci.* 11:119–192 (1985).
16. Xu, J., and Pope, S. B., *Combust. Flame,* in press (2000).
17. Barlow, R. S., The International Workshop on Measurement and Computation of Turbulent Non-Pre-

mixed Flames, http://www.ca.sandia.gov/tdf/Workshop.html, Sandia National Laboratories, CA.
18. Tacke, M. M., Cheng, T. C., Hassel, E. P., and Janicka, J., *Proc. Combust. Inst.* 26:169–175 (1996).
19. Landenfeld, T., Kremer, A., Hassel, E. P., and Janicka, J., *Proc. Combust. Inst.* 27:1023–1030 (1998).
20. Dally, B. B., Masri, A. R., Barlow, R. S., and Fiechtner, G. J., *Combust. Flame* 114:119–148 (1998).
21. Van Slooten, P. R., Jayesh, and Pope, S. B., *Phys. Fluids* 10(1):246 (1998).
22. Xu, J., and Pope, S. B., *J. Comput. Phys.* 152:192–230 (1999).
23. Masri, A. R., http://www.mech.eng.usyd.edu.au/research/energy/resources.html, University of Sydney, Australia.
24. Anand, M. S., Hsu, A. T., and Pope, S. B., *AIAA J.* 35(6):1143 (1997).
25. Subramaniam, S., and Pope, S. B., *Combust. Flame* 115:487–514 (1998).
26. Pope, S. B., *Combust. Theory Modelling* 1:41–63 (1997).
27. Saxena, V., and Pope, S. B., *Proc. Combust. Inst.* 27:1081–1086 (1998).
28. Xu, J., and Pope, S. B., Report FDA-99-06, Cornell University, Ithaca NY.
29. James, S., Anand, M. S., Razdan, M. K., and Pope, S. B., "*In Situ* Detailed Chemistry Calculations in Combustor Flow Analyses," Forty-Fourth ASME Gas Turbine and AeroEngine Technical Congress, Indianapolis, IN, June 1999.

COMMENTS

Carine Francois, SNECMA/CORIA, France. Did you try a computation on the same configuration without time averaging?

Author's Reply. No, we did not perform any computations without time averaging. It is mentioned in the paper that time averaging is an essential tool to reduce the statistical error and should be part of the computational procedure. It is important, however, to commence time averaging after a statistically stationary solution is reached.